Two-Dimensional Vanadium-Doped ZnO Nanosheet-Based Flexible Direct Current Nanogenerator

Manoj Kumar Gupta,[†] Ju-Hyuck Lee,[‡] Keun Young Lee,[†] and Sang-Woo Kim[†,‡,§,*]

[†]School of Advanced Materials Science and Engineering, [‡]SKKU Advanced Institute of Nanotechnology (SAINT), Center for Human Interface Nanotechnology (HINT), and [§]IBS Center for Integrated Nanostructure Physics, Institute for Basic Science (IBS), Sungkyunkwan University (SKKU), Suwon 440-746, Republic of Korea

ABSTRACT Here, we report the synthesis of lead-free single-crystalline two-dimensional (2D) vanadium(V)-doped ZnO nanosheets (NSs) and their application for high-performance flexible direct current (DC) power piezoelectric nanogenerators (NGs). The vertically aligned ZnO nanorods (NRs) converted to NS networks by V doping. Piezoresponse force microscopy studies reveal that vertical V-doped ZnO NS exhibit typical ferroelectricity with clear phase loops, butterfly, and well-defined hysteresis loops with a piezoelectric charge coefficient of up to 4 pm/V, even in 2D nanostructures. From pristine ZnO NR-based NGs, alternating current (AC)-type output current was observed, while from V-doped ZnO NS-based NGs, a DC-type output current density of up to 1.0 μAcm^{-2} was surprisingly obtained under the same vertical compressive force. The growth mechanism, ferroelectric behavior, charge inverted phenomena, and high piezoelectric output performance observed from the V-doped ZnO NS are discussed in terms of the formation of an ionic layer of [V(OH)$_4$$^-$], permanent electric dipole, and the doping-induced resistive behavior of ZnO NS.

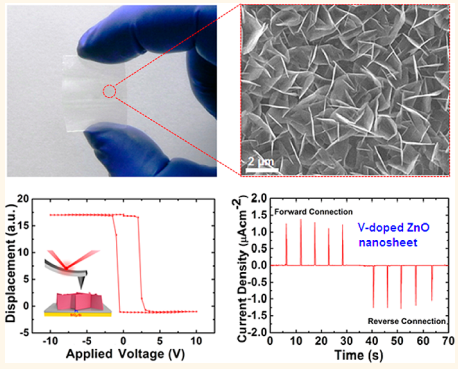

KEYWORDS: two-dimensional nanosheet · vanadium doping · ferroelectricity · piezoelectric nanogenerator · energy harvesting · direct current

Two-dimensional (2D) nanosheets (NSs) with atomic or molecular thickness and infinite planar dimensions are emerging as important new materials owing to their fascinating physics, unique properties, and potential applications in future electronics.[1,2] Recent research in 2D nanomaterial systems has strongly intensified due to progress in and observation of novel multifunctionalities in graphene, oxide, and chalcogenide NSs.[3−6] Particularly, oxide NSs have attracted exceptional attention due to their promising potential applications in areas ranging from catalysis to electronics.[7,8] ZnO nanostructures are of great scientific and technical interests due to their unique semiconducting, optical, and piezoelectric properties.[9] Recently, intensive studies have demonstrated new applications such as piezoelectric nanogenerators (NGs), self-powered piezotronic strain sensors, and Schottky contact-based nanosensors using 1D piezoelectric ZnO nanostructures such as nanowires, nanorods (NRs), and nanotubes.[10−13] However, despite the strong interests in 2D nanomaterials, the fabrication and characterization of 2D ZnO nanostructure-based piezoelectric NGs have rarely been investigated although power generation from the NG based on heterojunction of layered double hydroxide and 2D piezoelectric ZnO nanostructures on the nontransparent substrate has been reported very recently.[14]

The relatively lower piezoelectric coefficient and piezoelectric potential screening effect due to the numerous point defects and surface states acting as free charge carriers in pristine ZnO have restricted the realization of high-performance piezoelectric NGs and related applications.[10,15] Therefore, the development of NGs based on piezoelectric semiconductors such as ZnO, GaN, and CdS and with stable power output performance remains challenging.[16−18] Various methods such as thermal annealing, organic hybridization, and plasma treatment have been reported to improve the performance of ZnO-based NGs.[19−21] In contrast,

* Address correspondence to kimsw1@skku.edu.

Received for review July 5, 2013 and accepted September 4, 2013.

Published online September 04, 2013
10.1021/nn403428m

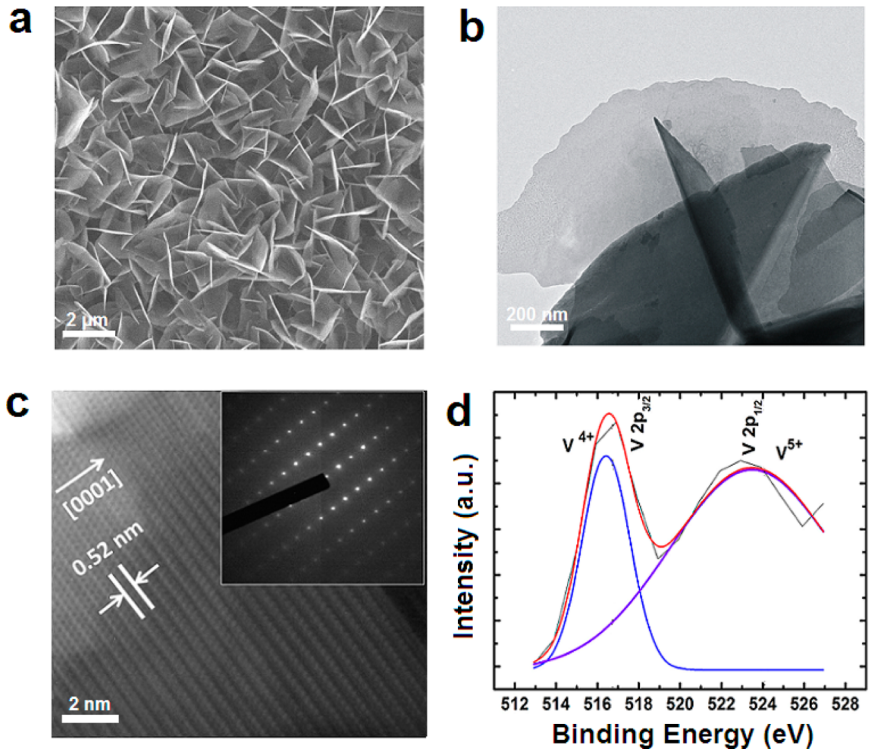

Figure 1. (a) FE-SEM image of 2D V-doped ZnO NS network. (b) TEM image of V-doped ZnO NS. (c) HR-TEM lattice image of V-doped ZnO NS. The inset shows a SAED pattern of NS, which confirms the single crystalline nature of V-doped ZnO. (d) XPS spectrum of V-doped ZnO NS, showing the presence of V $2p_{3/2}$ and V $2p_{1/2}$ state of vanadium in 2D V-doped ZnO NS.

doping in ZnO is a very common approach to tune its various properties such as electrical, optical, and piezoelectric properties.[22,23] In particular, the substitution of alkali/transition metal ions into Zn or O sites leads to various interesting properties such as ferroelectricity, ferromagnetism, and p-type conductivity.[22−25] For example, doping with vanadium(V) element in ZnO can abruptly increase its piezoelectric charge coefficient (d_{33}) value up to 125 pC/N, and these large piezoelectric response properties of V-doped ZnO are very promising for the fabrication of high-performance NGs.[26]

In spite many efforts, a direct current (DC) output NG remains very crucial for piezoelectric energy harvesting due to direct utilization of its generated power for various nanodevice applications. Unfortunately, however, only a few studies have reported the successful generation of DC output power from NGs.[10,16,27] Because most piezoelectric NGs generate alternating current (AC)-type charge output, the conversion of the signal from AC to DC requires a rectification circuit, which increases the total size of the power package and degrades its power. In the present work, we report the growth of lead-free single-crystalline ferroelectric V-doped 2D ZnO NSs and the realization of a high-performance flexible DC power output NG based on V-doped 2D ZnO NS networks for the first time.

RESULTS AND DISCUSSION

Large-scale single-crystalline V-doped ZnO NS networks on indium tin oxide (ITO)-coated polyethylene terephthalate (PET) substrates were synthesized through a cost-effective seed-assisted solution technique. Pristine undoped ZnO NRs on another ITO/PET substrate were grown *via* the same growth technique with no doping. The piezoelectric charge coefficient (d_{33}) and ferroelectric behavior of the vertically aligned V-doped ZnO NS networks were investigated with piezoresponse force microscope (PFM) measurements. Subsequently, we fabricated NGs using flexible gold/polyethersulfone (Au/PES) as the top electrode. Under compressive force, the ZnO NR-based NG generated AC-type piezoelectric signals, while the V-doped ZnO NS-based NGs generated pure DC-type large piezoelectric signals. Additionally, we discuss the mechanism on morphology evolution and inverted piezoelectric signals from AC to DC for V-doped ZnO NS networks in terms of geometry and doping in ZnO in detail.

The morphologies of the as-synthesized ZnO samples were characterized using field-emission scanning electron microscopy (FE-SEM) measurements. Figure 1a shows the FE-SEM image of the vertically grown V-doped ZnO NS networks. The average dimensions of these interwoven NSs were found in the range 900 nm−1.0 μm with a typical thickness of 15−20 nm. A low-resolution FE-SEM image of the grown 2D NS sample is also shown in Figure S1a, confirming the high uniform morphology

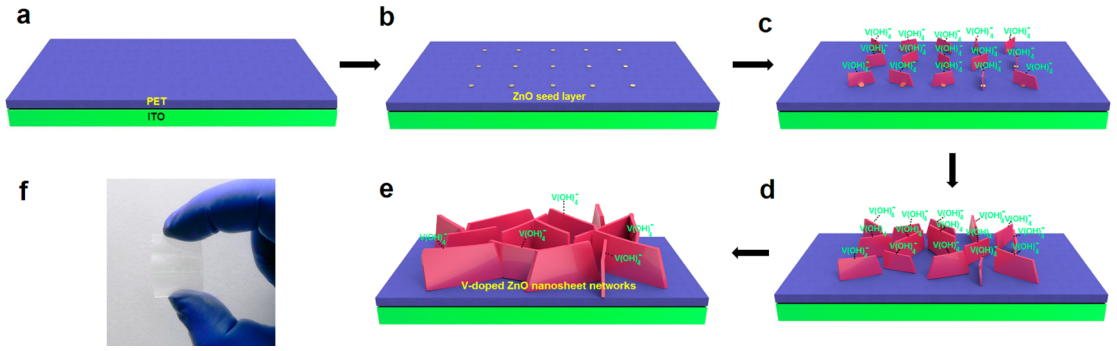

Figure 2. (a−e) Schematic diagrams for the growth mechanism of V-doped ZnO. The seed layer was deposited by spin coating on a bare ITO/PET substrate. $V(OH)_4^-$ ions are connected at the Zn^+ terminated surface, which blocks the 1D growth of V-doped ZnO. The resulting 2D formation was taken as a NS network. (f) Original image of vertically grown transparent and flexible V-doped ZnO NS on ITO/PET.

over a large area. As shown in the FE-SEM image, the vertically standing NSs were uniformly distributed in a high density on the surface of a flexible ITO/PET substrate and were connected to each other in the form of a network. A cross-sectional image of the vertically grown V-doped ZnO NS is shown in Figure S1b. A cross-sectional FE-SEM image of the vertically aligned pristine ZnO NRs on a flexible ITO/PET substrate is shown in Figure S2. The average diameter and length of the ZnO NRs were about 100 nm and 1.5 μm, respectively. The FE-SEM investigations revealed that V doping inverts the morphology of ZnO from 1D NRs into 2D NS networks. Wurzite structures of undoped ZnO NRs and V-doped ZnO NSs grown on ITO/PET substrates were confirmed by X-ray diffraction (XRD), and corresponding patterns are shown in Figure S3 of the Supporting Information.

Transmission electron microscope (TEM) was also applied to study the crystalline quality and size of the V-doped ZnO NS. A TEM image of a V-doped ZnO NS with an average dimension of around 1.0 μm is shown in Figure 1b. Further, Figure 1c presents a lattice-resolved high-resolution TEM image taken from the V-doped ZnO NS. The clearly resolved lattice fringe was calculated to be around 0.52 nm, in accordance with the [0001] plane of hexagonal ZnO crystal. A selected area electron diffraction (SAED) pattern in the inset of the Figure 1c is indexed as a hexagonal ZnO along the [0001] axis and also proves the single-crystalline nature of the V-doped ZnO NS. The V element incorporation into the ZnO lattice was also confirmed by energy dispersive spectrometer (EDS) analysis in which Zn, O, and V peaks were clearly detected (Figure S4).

In order to further confirm the V element and its electronic state in the doped ZnO NS, the sample was subjected to surface analysis by X-ray photoelectron spectroscopy (XPS). XPS spectra were recorded using Al Kα radiation. The wide scan XPS spectrum of the V-doped ZnO NS is shown in Figure S5. The high-resolved XPS spectrum in Figure 1d shows that the peaks at binding energy (BE) 516.84 and 524.14 eV were due to V 2p BE, which confirmed the V doping in the ZnO NS. Further, the first peak at BE of 516.84 eV corresponded to V $2p_{3/2}$ (V^{4+} valence state) and the second peak at higher BE of 524.14 eV corresponded to V $2p_{1/2}$, that is, a higher oxidation state of V (V^{5+} valence state).[28,29] The XPS spectrum thereby clearly indicated that the V-doped ZnO NS sample had V^{4+} and V^{5+} oxidation states of V in which the V^{5+} is incorporated into the crystal lattice of ZnO, while it is believed that the V^{4+} oxidation state of V atom arose due to presence of $[V(OH)_4^-]$ surface ions in the Zn^{2+} terminated V-doped ZnO NSs, as will be discussed in the growth mechanism section.

The formation mechanism of the NS network is shown schematically in Figure 2a−e. Initially, a seed solution of zinc acetate (0.04 M) was spin-coated on a bare flexible ITO-coated plastic substrate. Subsequently, zinc nitrate hexahydrate and hexamethylenetetramine (HMT) was used for the growth of V-doped ZnO NS. The main growth of V-doped ZnO NS was undertaken at 95 °C for 3 h (see Experiments and Methods). After the V doping, NR was completely converted into the 2D NS network by the following transition mechanisms. It is suggested that the formation of ZnO NR or NS is closely associated with OH^- ligands.[30,31] Generally, the growth habits of ZnO always directly decide the final shape of the crystal, which in turn is greatly influenced by its growth conditions. In an aqueous solution method, the growth of ZnO crystals is usually divided into two processes of nucleation and growth. The formation of pristine ZnO NRs can be described as the stacking of a number of alternate planes with tetrahedrally coordinated O^{2-} and Zn^{2+} ions along the *c*-axis. ZnO has positively charged (0001) and negatively charged $(000\bar{1})$ polar surfaces, while the (0001)-Zn terminated surface is chemically active and the $(000\bar{1})$-O terminated surface is inert. Preferential growth of ZnO along the *c*-axis is energetically favorable, which results in the formation 1D nanostructures.[32,33] During the growth of ZnO in the presence of HMT, negative ions (OH^- ions) are preferentially adsorbed to the (0001) plane and promote

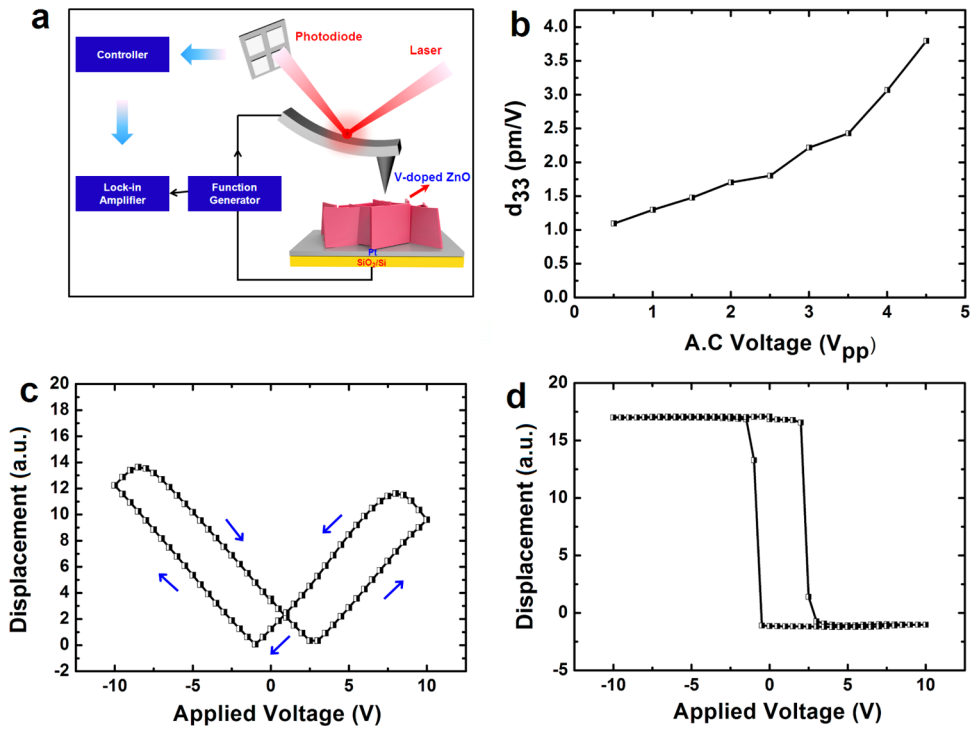

Figure 3. (a) Schematic diagram of PFM setup; (b) Piezoelectric response (d_{33}) results of the V-doped ZnO NS; (c) Amplitude-voltage butterfly loop; (d) Phase-voltage hysteresis loop, elucidating the 180° phase change.

crystal growth along the *c*-axis direction. This anisotropy growth is supported by the above-mentioned crystallographic habit of ZnO, so that 1D growth of the NRs in the [0001] direction is preferred.

On the other hand, in the growth procedure of the NS, Zn ions exist in the form of $Zn(OH)_2$ complex species serving as growth units for ZnO crystal growth in any direction. The excess OH^- ions are easily adsorbed on the positively charged (0001) surface and the growth along the [0001] direction is partially restricted. The extra hydroxide ions in the V-doped ZnO NS in this present case are supposed to originate from a doping source (V_2O_5, vanadium pentoxide). Because the V element undergoes chemical reactions under alkaline conditions in the presence of amine (HMT) and is supposed to form the vanadium hydroxide $[V(OH)_4^-]$, which can presumably bind to the positively charged Zn^{2+}-terminated (0001) polar surface of ZnO more strongly than to other nonpolar surfaces, the ZnO growth along the [0001] direction is effectively blocked, as shown schematically in Figure 2c–e. As a result, although the preferential direction of the *c*-axis is maintained as the crystal growth proceeds, the growth rate ratio of *c*-axis direction to other crystallographic directions decreases greatly due to the shielding effect of $[V(OH)_4^-]$ ions on the (0001) surface, which allows the lateral growth to occur in the form of 2D NS.[32−34] The original photo image of a flexible transparent 2D V-doped ZnO NS sample is shown in Figure 2f.

We used PFM to investigate the piezoelectric behavior of the V-doped ZnO NS sample. To measure the piezoelectric properties, we synthesized vertically aligned V-doped ZnO NS networks on a platinum (Pt)-coated SiO_2/Si substrate, as shown in Figure 3a. Before taking the PFM measurement, the morphology of the V-doped ZnO NS networks on SiO_2/Si was confirmed by FE-SEM (Figure S6). The electrical field of the PFM machine was applied to the tip with respect to substrate grounding. Using the PFM result, the d_{33} value of the 2D V-doped ZnO NS was calculated as 4 pm/V, as shown in Figure 3b, which was consistent with the reported d_{33} value of pure ZnO. However, the observed d_{33} value was low when compared to reported values of the V-doped ZnO thin film and the V-doped ZnO nanofiber.[22,26] Because pure ZnO possesses piezoelectricity due to the existence of the normal dipole moment and built-in polarization along its *c*-axis, and usually 1D ZnO nanostructures are the most desirable geometry to maximize the piezoelectric effect. On the other hand, maintaining piezoelectricity in 2D NS is a crucial and challenging task due to its 2D structure.

In the present study, we have shown that the piezoelectricity of V-doped ZnO NS is not only maintained by V doping, but also improved significantly. The high d_{33} value observed from the V-doped ZnO NS in the PFM study is attributed to the large polarization generation in V-doped ZnO NS due to the rotation of V–O bonds in addition to Zn–O bonds. Furthermore, V substitutes exist as V^{5+} ions in V-doped ZnO and have a higher positive charge than Zn^{2+} ions. Therefore, the noncollinear V–O bonds have a stronger polarity than the Zn–O bonds and rotate more easily in an applied electric field, which results high piezoelectric constant.[22]

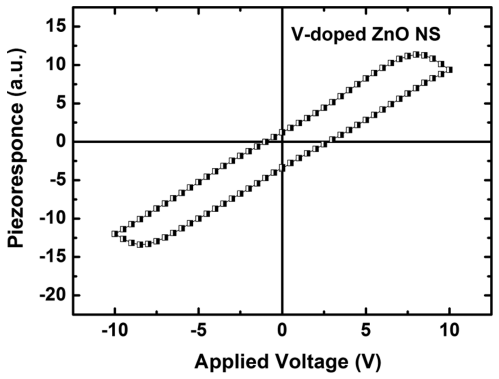

Figure 4. Piezoresponse–hysteresis curve of the V-doped ZnO NS, which confirms the ferroelectric behavior of V-doped ZnO NS.

In a further investigation based on the PFM measurements, V-doped ZnO NS showed butterfly loops and phase loops of the piezoelectric displacement as a function of the applied dc bias voltage from −10 to 10 V, as shown in Figure 3c and d, respectively. The 2D V-doped ZnO NS clearly shows a distinct hysteresis and 180° phase switching, which can be illustrated by their ferroelectric behavior.[35]

In addition, a well-defined piezoresponse hysteresis loop as shown in Figure 4 was also obtained from the V-doped ZnO NS, which proved its ferroelectric behavior. The origin of this ferroelectric behavior could be explained on the basis of the ionic radii difference between Zn^{2+} (0.74 Å) and the dopant ion V^{+} (0.60 Å). Due to this ionic size difference, V^{+} ions can occupy the off-centered positions, which leads to permanent local electric dipoles and, therefore, to the induction of ferroelectric behavior.[22,26] The insufficient insulating property in pure ZnO hindered the ferroelectric measurement because the applied electric field is screened by conduction electrons. However, Herng *et al.* recently reported vacancy-mediate pseudoferroelectricity in a high resistance state of pure ZnO thin film by a PFM study.[36] They reported that ferroelectric properties are not possible in pure ZnO due to the lack of off-centered position. Polarization switching is realized by the movement of the smaller Ti cations about the off-center position in typical ferroelectric $BaTiO_3$.[37] Therefore, in this present case, V^{+} ions can occupy the off-centered positions due to this ionic size difference, which leads to the formation of permanent local electric dipoles giving ferroelectric behavior in the 2D V-doped ZnO NS. This first demonstration of ferroelectricity in vertically aligned V-doped ZnO NSs offers exciting prospects for the fabrication of flexible and transparent, multiple information storage bits based on ZnO.

We subsequently fabricated a flexible NG device based on the grown 2D V-doped ZnO NS. The Au-coated PES top electrode was placed above the V-doped ZnO NS networks. The current–voltage curve taken from the V-doped ZnO NS-based NG device exhibited a clear Schottky behavior at the interface between the Au and the V-doped ZnO NSs. The V-doped ZnO NS was more electrically resistive than the undoped ZnO NR. Defect formation by V doping lowers the electron mobility, thereby further increasing the ZnO resistance. In addition, $[V(OH)_4^-]$ is absorbed on the surface of the ZnO NS, which correspondingly depletes the electron carriers and decreases the conductance of NS.[38,39] We measured the output current from the V-doped ZnO NS-based NG by applying a pushing force to the top of the NG in the vertical direction using a mechanical force stimulator. DC-type piezoelectric current output with an average value of 1.0 $\mu A \cdot cm^{-2}$ was obtained from the V-doped ZnO NS-based NG under vertical compressive force of 0.5 kgf, as shown in Figure 5a. On the other hand, AC-type piezoelectric current output with an average value of $\sim$10 $nA \cdot cm^{-2}$ was observed under direct compression under the same pushing force (Figure S7a,b). The output current from the V-doped ZnO NS-based NG was greatly enhanced compared to that from the undoped ZnO NR-based NG due to the network structure of NS. When a force is applied along the vertical direction, the stress can be transmitted through the network to all NSs under the force-applied area, which greatly enhances the NG performance. This dramatic increase in the current output may also be attributed to the high d_{33} value of V-doped ZnO NS, as discussed in the PFM section above, and to the highly resistive nature of V-doped ZnO NS with weak piezoelectric potential screening effect caused by the free electrons.

Figure 5b shows a schematic presentation of the as-fabricated V-doped ZnO NS-based NG. In the absence of any force, some negative ions are presented due to $[V(OH)_4^-]$. When the vertical pushing force is applied onto the V-doped NS-based NG, a negative piezoelectric potential is induced in the compressive side of NS (top side) and a positive piezoelectric potential becomes the other side (bottom side) of NS, as shown in Figure 5c. Therefore, piezoelectric potential-induced electrons are then transported *via* the external circuit to accumulate at the interface between the electrode and the side of NS with positive potential, which generates the positive pulse of current. When the external force is removed and the compressive strain is released, the piezoelectric potential disappears. The top side of V-doped ZnO NS is negatively charged due to $[V(OH)_4^-]$, even in the absence of any vertical force, which does not allow the back flow of accumulated electrons from the bottom electrode to the top electrode due to electrostatic repulsive force, as shown in Figure 5d. Therefore, no piezoelectric signal appears during the releasing of vertical force, which results in the perfect DC-type power generation from 2D V-doped ZnO NS-based NG. Therefore, continuous pushing and releasing of force on 2D V-doped NS-based NG creates DC-type piezoelectric signals. To verify that the measured signal

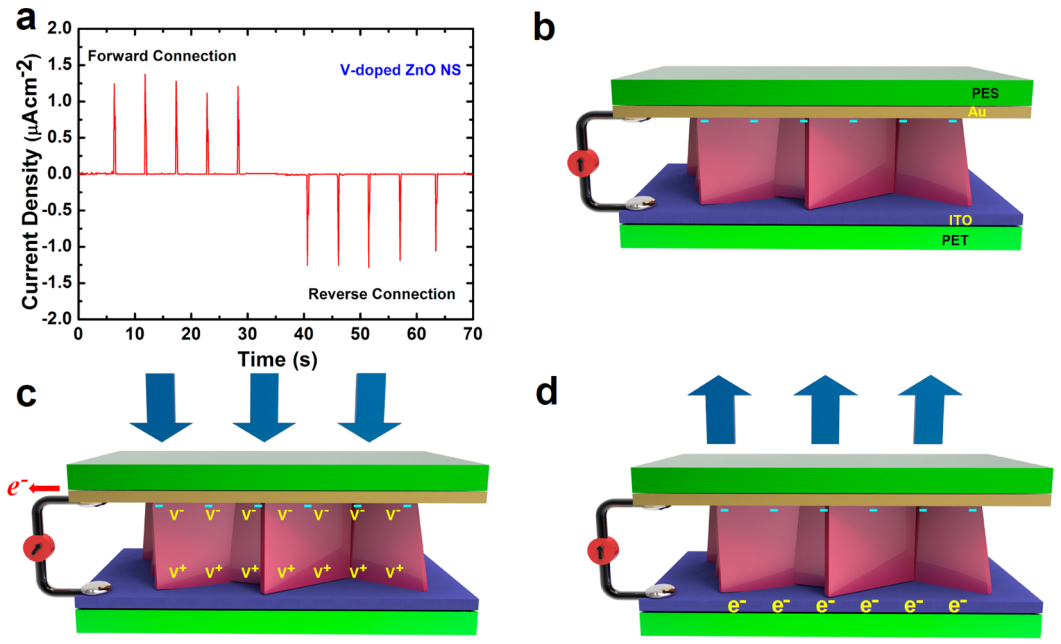

Figure 5. (a) Output current density generated from the NG fabricated with V-ZnO NS that presents DC-type charge generation. Schematic presentations of flexible integrated NG with an Au top electrode (Au-coated PES substrate) and proposed mechanisms. (b) As fabricated V-doped ZnO NS-based NG in the absence of any external force. (c) Piezoelectric potential induced electrons flow from the top electrode to the bottom electrode side through the external circuit under direct compression in the vertical direction. (d) As the compressive strain is released, the piezoelectric potential inside the NS instantly disappears and the accumulated electrons from the bottom electrode do not move to the top electrode due to the presence of negative ions at the top surface of NS, and subsequently, no signal is received during the release.

was generated by the NG device rather than the measurement system, we conducted a "switching-polarity" test. When the current meter was connected reversely, the pulses were also reversed.

CONCLUSIONS

In conclusion, 2D V-doped ZnO NS networks were prepared *via* the solution route on flexible ITO/PET substrates. The FE-SEM results revealed that the morphology of pure ZnO was altered from vertical 1D NR to vertical 2D NS due to V doping in the ZnO lattice. The growth mechanism was proposed on the basis of the $[V(OH)_4^-]$ passivating agent formed during the chemical reaction. The d_{33} value was 4 pm/V and a well-defined hysteresis curve was obtained, which confirmed the ferroelectric behavior of the grown 2D V-doped ZnO NS. V-doped ZnO NS generated a DC-type piezoelectric power output. This study provides not only a unique and facile way of growing highly efficient DC power-generating piezoelectric NGs based on V-doped ZnO NS but also a successful approach to grow transparent ferroelectric 2D ZnO NS using V doping. This unique DC power generation from piezoelectric NG will play an important role in the miniaturization of piezoelectric energy harvesting and storage devices by removing the need for a rectification circuit to convert the AC signal to DC signal. In addition, this facile synthesis method of transparent ferroelectric 2D ZnO NSs has potential applications in various devices such as nanosensors, transparent memory devices, piezotronic and piezophototronic devices, and self-powered switching devices.

EXPERIMENTS AND METHODS

Synthesis of Pure ZnO NRs and V-Doped ZnO NSs and Integration of NGs. 1D ZnO NRs and 2D V-doped ZnO NSs were synthesized using the aqueous solution method. Zinc acetate dehydrate $[Zn(CH_3COO)_2 \cdot 2H_2O$, 0.04 M] dissolved in ethanol (100 mL) at 90 °C was prepared as a high density seed solution. The seed solution was dropped onto the flexible ITO/PET substrate and spin-coated at 1000 rpm for 60 s. The spin-coated substrate, covered with a ZnO seed layer with high-density (0.04 M solution), was dried onto a hot template at 150 °C for 10 min. The coating and heating cycle was repeated six times. ZnO NR and NSs were formed on the ITO/PET substrate by immersion into an aqueous solution consisting of zinc nitrate hexahydrate $[Zn(NO_3)_2 \cdot 6H_2O$, 0.025 M], HMT (0.025 M), and deionized water (250 mL). The main growth of the ZnO NR and NSs occurred at 95 °C for 3 h. For V-doped ZnO NS, 0.001 M of V_2O_5 was added during the main growth of the ZnO separately in another beaker. To fabricate the NGs, a 100 nm thick Au layer was deposited on PES substrates using a thermal evaporator as the top electrode, which was integrated with pure ZnO NR and 2D V-doped ZnO NSs.

Characterization and Measurements. The synthesized pure and V-doped ZnO nanostructures underwent structural and crystallographic characterizations using XRD (Bruker D8 DISCOVER) with Cu Kα radiation (λ = 1.54 Å). The crystal shape and metal composition of these samples were probed with FE-SEM (Jeol JSM-6500F microscope). TEM images were obtained using a JEOL JEM-2100F microscope. A Keithley 6485 picoammeter and

2182A voltmeter were used to measure the low-noise output current and voltage generated from the piezoelectric NGs, respectively.

Conflict of Interest: The authors declare no competing financial interest.

Acknowledgment. This work was financially supported by Basic Science Research Program through the National Research Foundation (NRF) of Korea Grant funded by the Ministry of Science, ICT and Future Planning (2012R1A2A1A01002787, 2010-0019086, 2009-0083540), and the Energy International Collaboration Research and Development Program of the Korea Institute of Energy Technology Evaluation and Planning (KETEP) funded by the Ministry of Knowledge Economy (MKE; 2011-8520010050).

Supporting Information Available: Low-resolution FE-SEM image of V-doped ZnO NS and cross-sectional FE-SEM image of V-doped ZnO NS networks. Cross-sectional FE-SEM image of pure ZnO NRs. EDS spectrum of the V-doped ZnO NSs. Wide scan XPS pattern of V-doped ZnO NS on ITO/PET substrate. FE-SEM image of 2D V-doped ZnO NS networks on a Pt/SiO_2/Si substrate. Schematic diagram of flexible ZnO NR-based NG and piezoelectric output current output from under a vertical compressive force of 0.5 kgf. This material is available free of charge *via* the Internet at http://pubs.acs.org.

REFERENCES AND NOTES

1. Service, R. F. Carbon Sheets an Atom Thick Give Rise to Graphene Dreams. *Science* **2009**, *324*, 875–877.
2. Lee, K. H.; Shin, H. J.; Lee, J.; Lee, I.; Kim, G. H.; Choi, J. Y.; Kim, S.-W. Large-Scale Synthesis of High-Quality Hexagonal Boron Nitride Nanosheets for Large-Area Graphene Electronics. *Nano Lett.* **2012**, *12*, 714–718.
3. Huang, X.; Zeng, Z.; Fan, Z.; Liu, J.; Zhang, H. Graphene-Based Electrodes. *Adv. Mater.* **2012**, *24*, 5979–6004.
4. Bitounis, D.; Boucetta, H. A.; Hong, B. H.; Min, D. H.; Kostarelos, K. Prospects and Challenges of Graphene in Biomedical Applications. *Adv. Mater.* **2013**, *25*, 2258–2268.
5. Lee, H. S.; Min, S. W.; Chang, Y. G.; Park, M. K.; Nam, T.; Kim, H.; Kim, J. H.; Ryu, S.; Im, S. MoS_2 Nanosheet Phototransistors with Thickness-Modulated Optical Energy Gap. *Nano Lett.* **2012**, *12*, 3695–3700.
6. Li, C.; Huang, L.; Snigdha, G. P.; Yu, Y.; Cao, L. Role of Boundary Layer Diffusion in Vapor Deposition Growth of Chalcogenide Nanosheets: The Case of GeS. *ACS Nano* **2012**, *6*, 8868–8877.
7. Tagusagawa, C.; Takagaki, A.; Hayashi, S.; Domen, K. Characterization of $HNbWO_6$ and $HTaWO_6$ Metal Oxide Nanosheet Aggregates As Solid Acid Catalysts. *J. Phys. Chem. C* **2009**, *113*, 7831–7837.
8. Osada, M.; Sasaki, T. Exfoliated Oxide Nanosheets: New Solution to Nanoelectronics. *J. Mater. Chem.* **2009**, *19*, 2503–2511.
9. Wang, Z. L.; Kong, X. Y.; Ding, Y.; Gao, P.; Hughes, W. L.; Yang, R.; Zhang, Y. Semiconducting and Piezoelectric Oxide Nanostructures Induced by Polar Surfaces. *Adv. Funct. Mater.* **2004**, *14*, 943–956.
10. Park, H. K.; Lee, K. Y.; Seo, J.-S.; Jeong, J. A.; Kim, H. K.; Choi, D.; Kim, S.-W. Charge- Generating Mode Control in High-Performance Transparent Flexible Piezoelectric Nanogenerators. *Adv. Funct. Mater.* **2011**, *21*, 1187–1193.
11. Zhou, J.; Gu, Y.; Fei, P.; Mai, W.; Gao, Y.; Yang, R.; Bao, G.; Wang, Z. L. Flexible Piezotronic Strain Sensor. *Nano Lett.* **2008**, *8*, 3035–3040.
12. Pan, C.; Yu, R.; Niu, S.; Zhu, G.; Wang, Z. L. Piezotronic Effect on the Sensitivity and Signal Level of Schottky Contacted Proactive Micro/Nanowire Nanosensors. *ACS Nano* **2013**, *7*, 1803–1810.
13. Xi, Y.; Song, J.; Xu, S.; Yang, R.; Gao, Z.; Hu, C.; Wang, Z. L. Growth of ZnO Nanotube Arrays and Nanotube Based Piezoelectric Nanogenerators. *J. Mater. Chem.* **2009**, *19*, 9260–9264.
14. Kim, K. H.; Kumar, B.; Lee, K. Y.; Park, H. K.; Lee, J. H.; Lee, H. H.; Jun, H.; Lee, D.; Kim, S.-W. Piezoelectric Two-Dimensional Nanosheets/Anionic Layer Heterojunction for Efficient Direct Current Power Generation. *Sci. Rep.* **2013**, *3*, 2017.
15. Gao, Y.; Wang, Z. L. Equilibrium Potential of Free Charge Carriers in a Bent Piezoelectric Semiconductive Nanowire. *Nano Lett.* **2009**, *9*, 1103–1110.
16. Kumar, B.; Lee, K. Y.; Park, H.-K.; Chae, S. J.; Lee, Y. H.; Kim, S.-W. Controlled Growth of Semiconducting Nanowire, Nanowall, and Hybrid Nanostructures on Graphene for Piezoelectric Nanogenerators. *ACS Nano* **2011**, *5*, 4197–4204.
17. Huang, C. T.; Song, J.; Lee, W. F.; Ding, Y.; Gao, Z.; Hao, Y.; Chen, L. J.; Wang, Z. L. GaN Nanowire Arrays for High-Output Nanogenerators. *J. Am. Chem. Soc.* **2010**, *132*, 4766–4771.
18. Lin, Y. F.; Song, J.; Ding, Y.; Lu, S. Y.; Wang, Z. L. Piezoelectric Nanogenerator Using Cds Nanowires. *Appl. Phys. Lett.* **2008**, *92*, 022105.
19. Hu, Y.; Lin, L.; Zhang, Y.; Wang, Z. L. Replacing a Battery by a Nanogenerator with 20 V Output. *Adv. Mater.* **2012**, *24*, 110–114.
20. Pham, T. T.; Lee, K. Y.; Lee, J.-H.; Kim, K. H.; Shin, K. S.; Gupta, M. K.; Kumar, B.; Kim, S.-W. Reliable Operation of a Nanogenerator under Ultraviolet Light *via* Engineering Piezoelectric Potential. *Energy Environ. Sci.* **2013**, *6*, 841–846.
21. Lee, K. Y.; Kumar, B.; Seo, J.-S.; Kim, K.-H.; Sohn, J. I.; Cha, S. N.; Choi, D.; Wang, Z. L.; Kim, S.-W. p-Type Polymer-Hybridized High-Performance Piezoelectric Nanogenerators. *Nano Lett.* **2012**, *12*, 1959–1964.
22. Chen, Y. Q.; Zheng, X. J.; Feng, X. The Fabrication of Vanadium-Doped ZnO Piezoelectric Nanofiber by Electrospinning. *Nanotechnology* **2010**, *21*, 055708–4.
23. Radovanovic, P. V.; Gamelin, D. R. High-Temperature Ferromagnetism in Ni^{2+}-Doped ZnO Aggregates Prepared from Colloidal Diluted Magnetic Semiconductor Quantum Dots. *Phys. Rev. Lett.* **2003**, *19*, 157202.
24. Tsukazaki, A.; Ohtomo, A.; Onuma, T.; Ohtani, M.; Makino, T.; Sumiya, M.; Ohtani, K.; Chichibu, S. F.; Fuke, S.; Segawa, Y.; et al. Repeated Temperature Modulation Epitaxy for p-Type Doping and Light-Emitting Diode Based on ZnO. *Nat. Mater.* **2005**, *4*, 42–46.
25. Yang, Y.; Pradel, K. C.; Jing, Q.; Wu, J. M.; Zhang, F.; Zhou, Y.; Zhang, Y.; Wang, Z. L. Thermoelectric Nanogenerators Based on Single Sb-Doped ZnO Micro/Nanobelts. *ACS Nano* **2012**, *6*, 6984–6989.
26. Yang, Y. C.; Song, C.; Wang, X. H.; Zeng, F.; Pan, F. Giant Piezoelectric d_{33} Coefficient in Ferroelectric Vanadium Doped ZnO Films. *Appl. Phys. Lett.* **2008**, *92*, 012907.
27. Wang, X.; Song, J.; Liu, J.; Wang, Z. L. Direct-Current Nanogenerator Driven by Ultrasonic Waves. *Science* **2007**, *316*, 102–105.
28. Liu, H.; Wu, Y.; Zhang, J. A New Approach toward Carbon-Modified Vanadium-Doped Titanium Dioxide Photocatalysts. *ACS Appl. Mater. Interfaces* **2011**, *3*, 1757–1764.
29. Bondarenka, V.; Grebinskij, S.; Kaciulis, S.; Mattogno, G.; Mickevicius, S.; Vardauskas, H.; Volkov, V.; Zakharova, G. XPS Study of Vanadium-Yttrium Hydrates. *J. Electron Spectrosc. Relat. Phenom.* **2001**, *120*, 131–135.
30. Cao, B.; Cai, W. From ZnO Nanorods to Nanoplates: Chemical Bath Deposition Growth and Surface-Related Emissions. *J. Phys. Chem. C* **2008**, *112*, 680–685.
31. Sun, Y.; Riley, D. J.; Ashfold, M. N. R. Mechanism of ZnO Nanotube Growth by Hydrothermal Methods on ZnO Film-Coated Si Substrates. *J. Phys. Chem. B* **2006**, *110*, 15186–15192.
32. Vohs, J. M.; Barteau, M. A. Conversion of Methanol, Formaldehyde and Formic Acid on the Polar Faces of Zinc Oxide. *Surf. Sci.* **1986**, *176*, 91–114.
33. Dulub, O.; Diebold, U.; Kresse, G. Novel Stabilization Mechanism on Polar Surfaces: ZnO(0001)-Zn. *Phys. Rev. Lett.* **2003**, *90*, 016102.
34. Ye, C.; Bando, Y.; Shen, G.; Golberg, D. Thickness-Dependent Photocatalytic Performance of ZnO Nanoplatelets. *J. Phys. Chem. B* **2006**, *110*, 15146–15151.
35. Wang, Z.; Hu, J.; Yu, M. F. One-Dimensional Ferroelectric Monodomain Formation in Single Crystalline $BaTiO_3$ Nanowire. *Appl. Phys. Lett.* **2006**, *89*, 263119.
36. Herng, T. S.; Kumar, A.; Ong, C. S.; Feng, Y. P.; Lu, Y. H.; Zeng, K. Y.; Ding, J. Investigation of the Non-Volatile Resistance Change in Noncentrosymmetric Compounds. *Sci. Rep.* **2012**, *2*, 587.

37. Callister, W. D.; Rethwisch, D. G. *Materials Science and Engineering*; Wiley: New York, 2010.
38. Li, Q. H.; Gao, T.; Wang, Y. G.; Wang, T. H. Adsorption and Desorption of Oxygen Probed from ZnO Nanowire Films by Photocurrent Measurements. *Appl. Phys. Lett.* **2005**, *86*, 123117.
39. Weissenberger, D.; Dürrschnabel, M.; Gerthsen, D.; Willard, F. P.; Reiser, A.; Prinz, G. M.; Feneberg, M.; Thonke, K.; Sauer, R. Conductivity of Single ZnO Nanorods after Ga Implantation in a Focused-Ion-Beam System. *Appl. Phys. Lett.* **2007**, *91*, 132110.